

## Supporting Information

### Visible and Infrared Photodetector based on $\gamma$ -InSe/Ge van der Waals Heterojunction For Polarized Detection and Imaging

Baoxiang Yang<sup>1</sup>, Wei Gao<sup>1\*</sup>, Hengyi Li<sup>1</sup>, Peng Gao<sup>1</sup>, Mengmeng Yang<sup>1</sup>, Yuan Pan<sup>1</sup>,

Chuanglei Wang<sup>1</sup>, Yani Yang<sup>1</sup>, Nengjie Huo<sup>1</sup>, Zhaoqiang Zheng<sup>2\*</sup>, Jingbo Li<sup>1\*</sup>

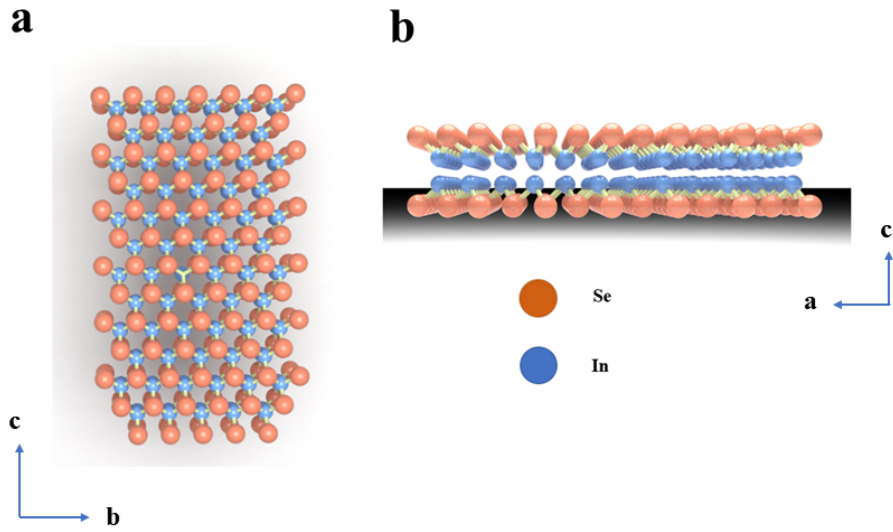
<sup>1</sup> School of Semiconductor Science and Technology, Guangdong Provincial Key  
Laboratory of Chip and Integration Technology, South China Normal University,  
Guangzhou 528225, P. R. China

<sup>2</sup> School of Materials and Energy, Guangdong University of Technology, Guangzhou  
510006, P. R. China.

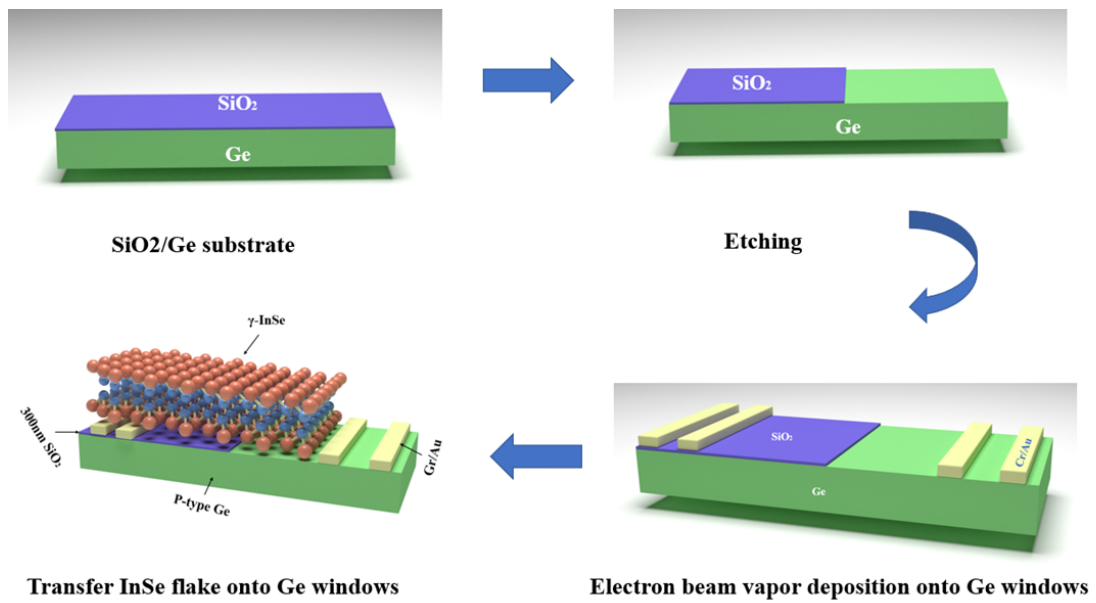
**\*Corresponding authors:** Wei Gao, Email: gaowei317040@m.scnu.edu.cn

Zhaoqiang Zheng, Email: zhengzhq5@mail2.sysu.edu.cn

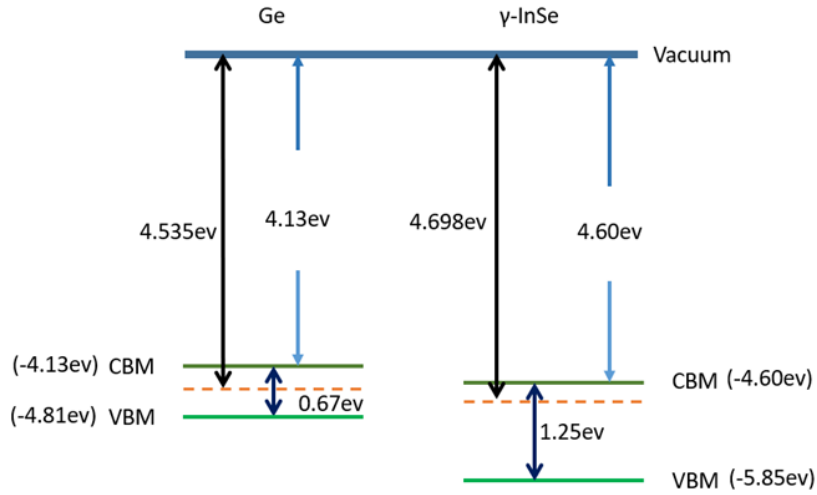
Jingbo Li, Email: jbli@m.scnu.edu.cn



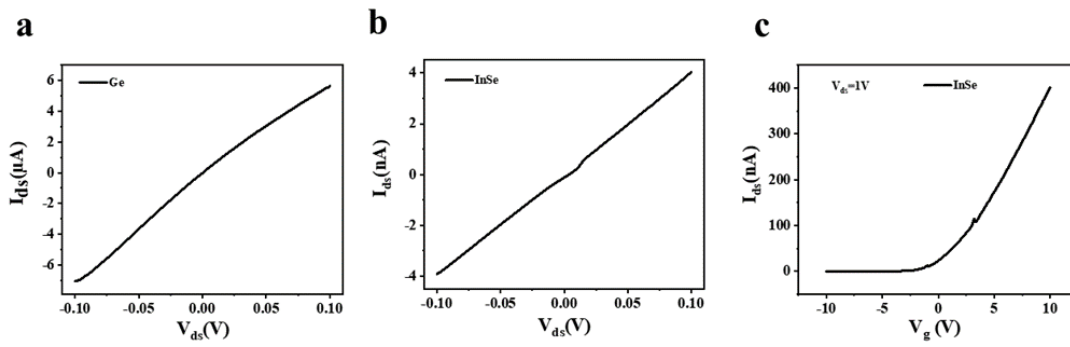
**Figure S1.** The lattice structure of 2D  $\gamma$ -InSe nanosheet. (a) the b-axis views and (b) the a-axis views of InSe atomic structure.



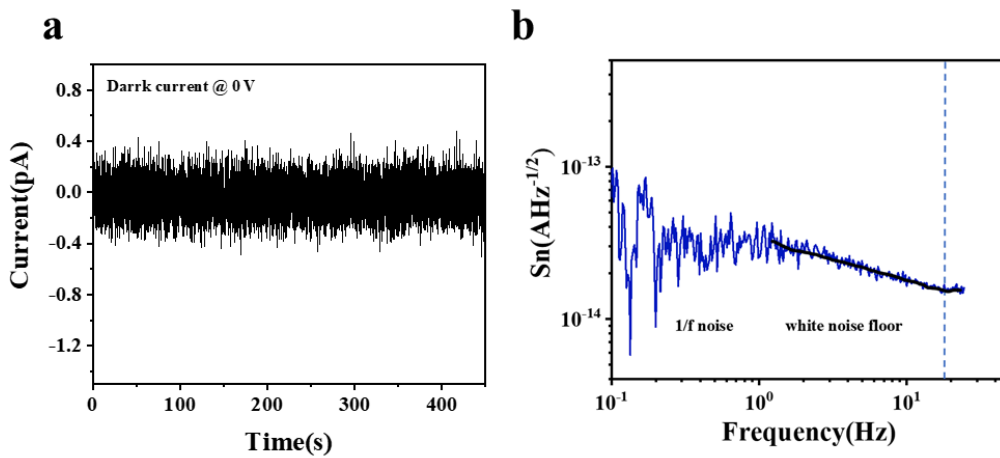
**Figure S2.** Schematic illustration for the fabrication process of InSe/Ge van der Waals heterojunction photodiode.



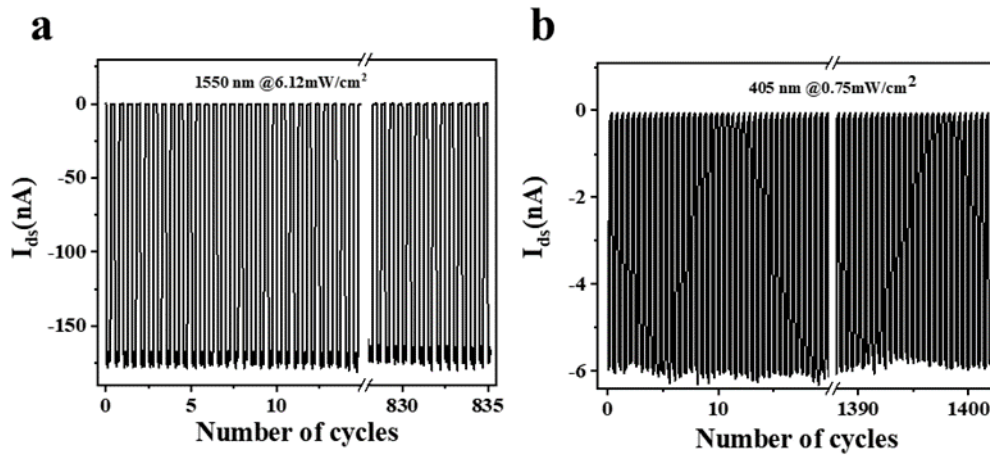
**Figure S3.** Band diagram of Ge and InSe before contact.



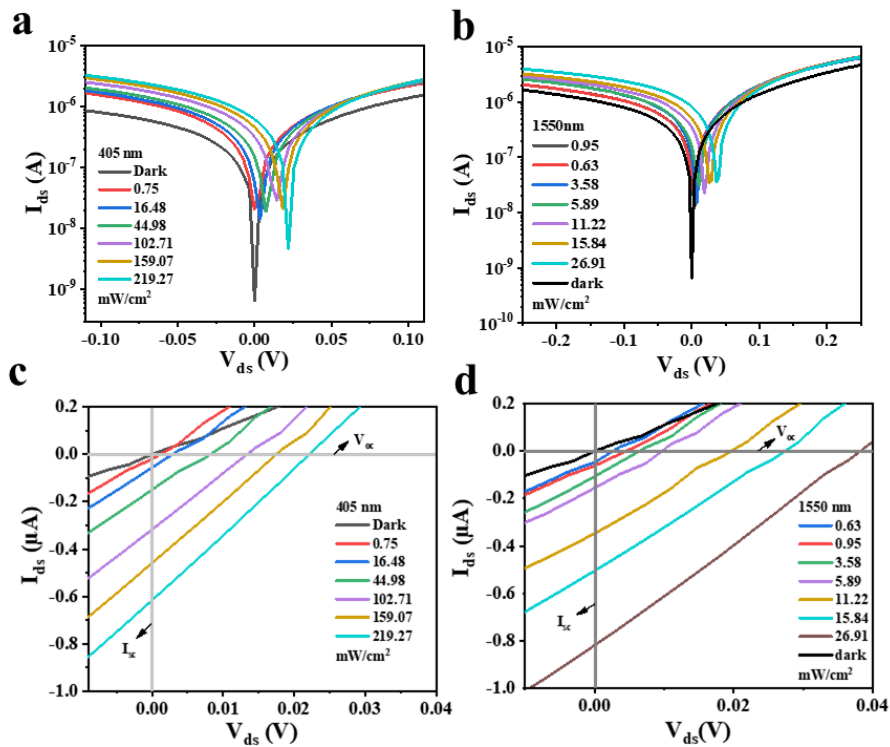
**Figure S4.** (a, b)  $I_{ds}$ - $V_{ds}$  curves of individual Ge and InSe based devices, respectively. (c). Transfer curve of  $\gamma$ -InSe.



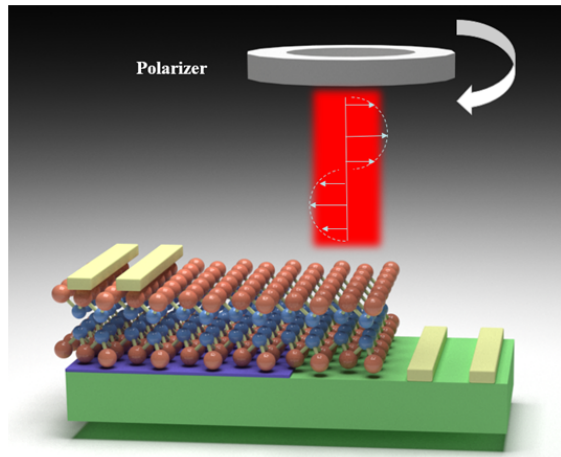
**Figure S5.** (a) Dark current at  $V_{ds} = 0$  V and (b) Noise spectral density as a function of frequency at  $V_{ds} = 0$  V



**Figure S6.** (a, b). The long-term photo-response curves at zero bias under 1550 and 405 nm light irradiation.



**Figure S7.**  $I_{ds}$ - $V_{ds}$  of the device with the dark and various infrared light power at 1550 nm (a), 405 nm (b). (c), (d) Enlarged  $I_{ds}$ - $V_{ds}$  curves of the heterojunction device in dark and under 405 and 1550 nm with various light power densities.

**a**

**Figure S8.** Schematic diagram of the test system of the polarization photodetector.

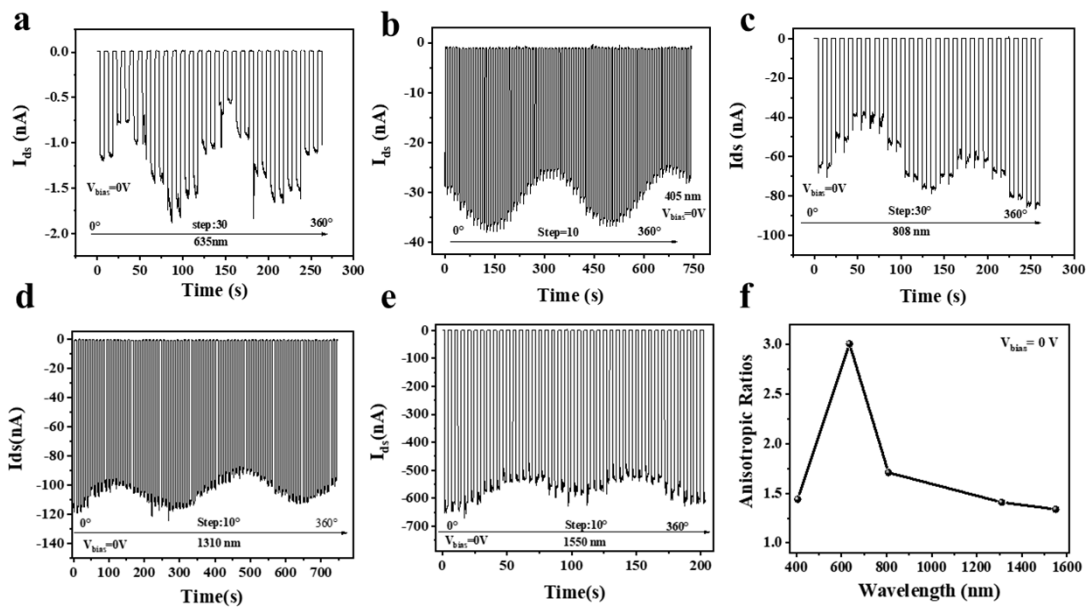


**Figure S9.** (a,b,c,d,e) The time resolved photocurrent of Ge/InSe heterojunction under polarized light with varying polarization angle from  $0^\circ$  to  $360^\circ$  under 635 nm (light power: 0.024 mW), 405 nm (light power: 1.93 mW), 808 nm (light power: 0.3 mW), 1310 nm (light power: 1.11 mW) and 1550 nm (light power: 6.67 mW) light illumination. (f) indicates the polarization ratio versus wavelength.

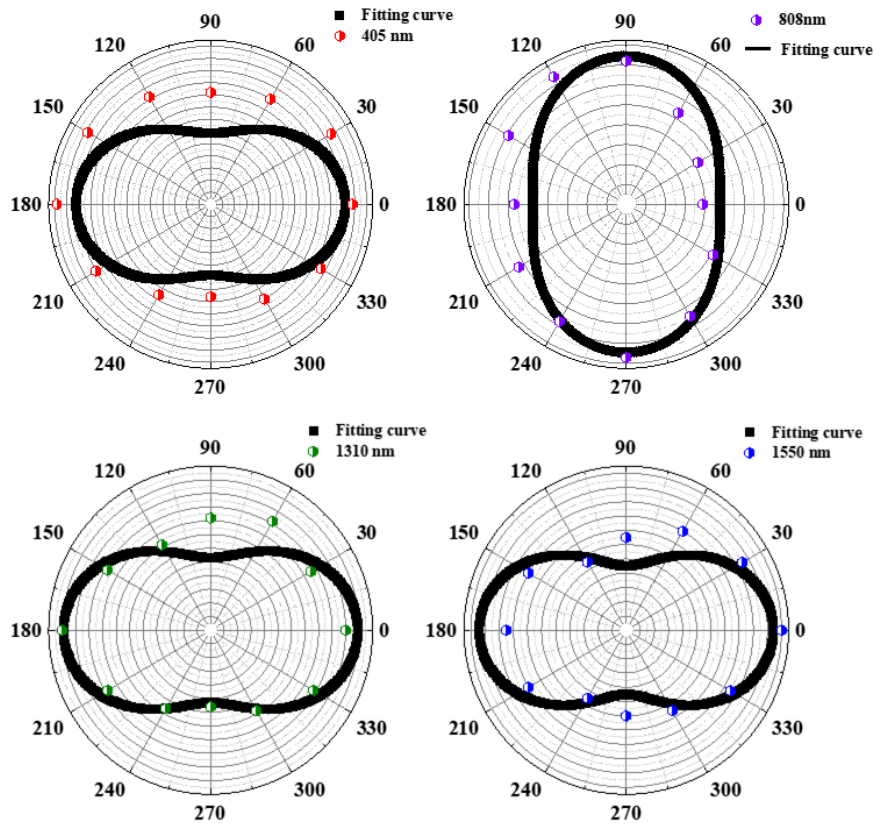


**Figure S10.** (a,b,c,d) Polar plots of the normalized photocurrents of Ge/InSe heterojunctions at 405, 808, 1310 and 1550 nm at zero bias voltage.

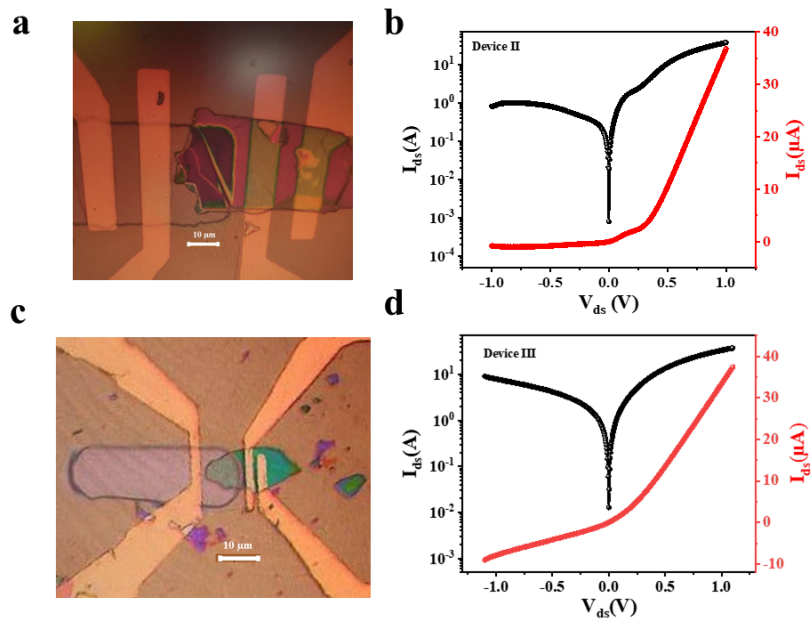


**Figure S11.** Optical image of (a) Device II and (c) Device III.  $I_{ds}$ - $V_{ds}$  curves of (b) Device II and (d) Device III in darkness.

**Table S1.** Comparison of device performance of the present device with other similar Ge-based photodetectors.

Device	$\lambda$ (nm)	Self-power	Polarization sensitivity	R(A/W)	D*(Jones)	Raise/fall time( $\mu$ s)	ref
InSe/Ge	405-1550	yes	3.01	9.82(1550nm) 0.8(405nm)	$5.4 \times 10^{11}$ (1550nm) $4.8 \times 10^{10}$ (405nm)	46/32	This work
Graphene/Ge	1200-1600	yes	/	0.051	$1.38 \times 10^1$ <sub>0</sub>	23/108	1
PtSe <sub>2</sub> /Ge	405-2200	yes	/	0.602	$6.31 \times 10^1$ <sub>1</sub>	7.42/16.71	2
PdSe <sub>2</sub> /Ge	<2200	yes	/	0.53	$1.45 \times 10^1$ <sub>1</sub>	25.4/38.5	3
WS <sub>2</sub> /AlO <sub>x</sub> /Ge	200-4600	yes	/	0.6345	$4.3 \times 10^{11}$	9.8/12.7	4
WSe <sub>2</sub> /Ge	520-1550	yes	/	1.3	$2.5 \times 10^{10}$	30/5	5
MoTe <sub>2</sub> /Ge	915-1550	yes	/	0.19	$1.15 \times 10^1$ <sub>1</sub>	8/6	6

## References

- 1 L.-H. Zeng, M.-Z. Wang, H. Hu, B. Nie, Y.-Q. Yu, C. Wu, L. Wang, J.-G. Hu, C. Xie, F.-X. Liang and L.-B. Luo, Monolayer graphene/germanium Schottky junction as high-performance self-driven infrared light photodetector, *ACS applied materials & interfaces*, 2013, **5**, 9362–9366.
- 2 L. Wang, J.-J. Li, Q. Fan, Z.-F. Huang, Y.-C. Lu, C. Xie, C. Wu and L.-B. Luo, A high-performance near-infrared light photovoltaic detector based on a multilayered PtSe<sub>2</sub>/Ge heterojunction, *J. Mater. Chem. C*, 2019, **7**, 5019–5027.
- 3 L.-B. Luo, Di Wang, C. Xie, J.-G. Hu, X.-Y. Zhao and F.-X. Liang, PdSe<sub>2</sub> Multilayer on Germanium Nanocones Array with Light Trapping Effect for Sensitive Infrared Photodetector and Image Sensing Application, *Adv Funct Materials*, 2019, **29**, 1900849.
- 4 Di Wu, J. Guo, C. Wang, X. Ren, Y. Chen, P. Lin, L. Zeng, Z. Shi, X. J. Li, C.-X. Shan and J. Jie, Ultrabroadband and High-Detectivity Photodetector Based on WS<sub>2</sub>/Ge Heterojunction through Defect Engineering and Interface Passivation, *ACS nano*, 2021, **15**, 10119–10129.
- 5 C. H. Lee, Y. Park, S. Youn, M. J. Yeom, H. S. Kum, J. Chang, J. Heo and G. Yoo, Design of p-WSe<sub>2</sub>/n-Ge Heterojunctions for High-Speed Broadband Photodetectors, *Adv Funct Materials*, 2022, **32**, 2107992.
- 6 W. Lei, X. Wen, L. Yang, P. Zhang, G. Cao, F. Zhuge, Y. Zhang, H. Chang and W. Zhang, Vertical MoTe<sub>2</sub>/Ge Heterojunction Photodiode for 1550-nm Near-Infrared Photodetection, *IEEE Trans. Electron Devices*, 2022, 1–5.

